International Journal of Nanomedicine

Dovepress
Taylor & Francis Group

Open Access Full Text Article

ORIGINAL RESEARCH

LIFU (Low-Intensity Focused Ultrasound) Activated Tumor-Starvation/Oxidative-Stress Combined Therapy for Treating Retinoblastoma

Luya Quan[1–3], Mengzhu Wang[2], Zhigang Wang[2], Zhiyu Du[3]

[1]Department of Ophthalmology, The Guizhou Provincial People's Hospital, Guiyang, Guizhou, 550002, People's Republic of China; [2]Department of Ultrasound, Chongqing Key Laboratory of Ultrasound Molecular Imaging, The Second Affiliated Hospital of Chongqing Medical University, Chongqing, 400010, People's Republic of China; [3]Department of Ophthalmology, The Second Affiliated Hospital of Chongqing Medical University, Chongqing, 400010, People's Republic of China

Correspondence: Zhiyu Du, Department of Ophthalmology, The Second Affiliated Hospital of Chongqing Medical University, Chongqing, 400010, People's Republic of China, Email dr.duzhiyu@163.com

Purpose: To overcome the limitations of traditional therapies in treating retinoblastoma, like low efficiency, systematic toxicity and poor biocompatibility.

Materials and Methods: PPFG (PLGA-PFH-Fe_3O_4-GOx) nanoparticles were synthesized by ultrasound double emulsification method and characterized by dynamic laser scattering, ultraviolet spectrometry, confocal laser scanning microscopy (CLSM), transmission electron microscopy (TEM) and scanning electron microscopy (SEM). Phase transition by low-intensity focused ultrasound (LIFU) was observed by microscope and ultrasound imaging. Cellular uptake was compared between Y79 and HUVEC cells. ROS production was detected by 2′,7′-dichlorofluorescin diacetate (DCFH-DA). Cell apoptosis was detected by flow cytometry. In vivo therapeutic effects were verified by tumor volume, HE staining, TUNEL and PCNA staining. The in vivo bio-safety was detected by serum biochemistry.

Results: PPFG NPs possesses good stability, biocompatibility and tumor-preferred uptake, with a core-shell spherical structure and an average size of 255.6nm which increases to over 100μm under LIFU irradiation. LIFU was utilized as a stimuli, by which PPFG NPs undergoes a sequential reaction starting with phase transition of PFH causing the release of the oxygen carried by PFH and GOx/SPIO carried by PPFG NPs, followed by the supplemented oxygen facilitating the enzymatic activity of glucose consumption by GOx in tumor cells (tumor starvation), the H_2O_2 produced during the enzymatic activity can further participate in SPIO NPs-mediated Fenton reaction (CDT), generating massive ROS. The continuously generated ROS together with the cut down of tumor nutrients by GOx effectively inhibited the progression of tumors, and synergistically enhanced ROS production together with tumor starvation promoted cell apoptosis and ultimately kills the tumour cells. No off-site injuries was detected in other major organs.

Conclusion: In this study, PPFG nanoparticles were synthesized to conduct LIFU-triggered combinational therapy on the basis of the cascade reaction among PFH, GOx and SPIO to treat retinoblastoma in vitro/vivo. It showed great potentials in combating retinoblastoma.

Keywords: retinoblastoma, ADV, LIFU, glucose oxidase, chemodynamic therapy

Introduction

Retinoblastoma (RB) is the most common primary intraocular malignant tumor in children (infants and young children), with a global prevalence of approximately 1/16,000–1/18,000 live births, which is equivalent to about 8,000–9,000 new cases annually and accounted for 3–4% of total pediatric malignancies.[1–4] It could cause detrimental effects without effective early treatment, including blindness, secondary non-ocular tumors, and mortality.[5] Traditional therapies for retinoblastoma, such as radiotherapy (including local radiation, also known as episcleral plaque radiotherapy, and external beam radiotherapy (EBRT)), chemotherapy (including intra-venous, intra-arterial, sub-conjunctival, and intravitreal chemotherapy), transpupillary thermotherapy, laser photocoagulation, cryotherapy, gene therapy, and enucleation.[4,6–8] The therapeutic effects of these traditional

Received: 27 November 2024
Accepted: 27 February 2025
Published: 3 April 2025

Graphical Abstract

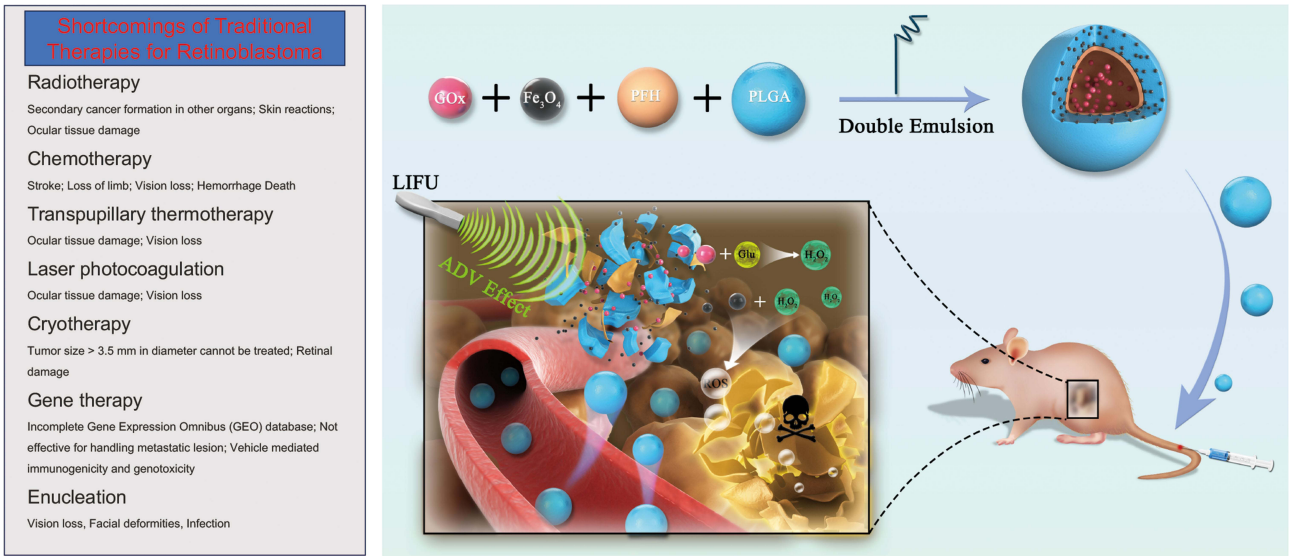

methods are limited due to potential side effects, including increased risk of secondary tumors, drug resistance, unstable efficacy and high toxicity, which may affect psychological growth and even cause death of children. Treatments with high efficiency and safety are urgently in demand.[8,9]

With the fast development of nanotechnology, problems faced by traditional therapies can be addressed by exploiting bio-materials to accomplish nanodrug deliver.[4,10–13] The unique enhanced permeability and retention (EPR) effect allows nanoparticles to achieve tumor-targeted bio-distribution and enhance drug delivery efficiency in tumors, which reduces the toxicity and side effects, increases drug utilization efficiency, and diversifies therapeutic approaches for retinoblastoma.[4,12] Previous researches have reported that Nanoplatform FA-DOX-ICG-PFP@Lip designed by Li et al and magnetic hollow mesoporous gold nanocages (namely AuNCs) designed by Wang et al exhibited significant tumour-inhibiting effects.[14,15] Nevertheless, poor stability of liposomes, the biodegradability and moderate cytotoxic profile of complex metal nanoplatform remain concerns.

Over the past decades, nanozyme has been playing an important role in cancer therapy, considering its good stability, low production cost and simple preparation procedures.[16–20] Some of the enzymatically active substances can be encapsulated in nanomaterials to form nano-enzymatic complexes. Among them, glucose oxidase (GOx), due to the unique catalytic efficacy and inherent biocompatibility/biodegradability, has attracted much attention in nano-biomedicine.[21–25] On the one hand, glucose oxidase reacts with endogenous glucose, which consumes glucose in tumor cells and cuts off the nutritional source of tumor tissues, generates tumor starvation response and thus inhibits tumor growth. On the other hand, the efficient catalytic ability of GOx converses intratumoral glucose into abundant H_2O_2, and the generated H_2O_2 effectively compensates for the lack of endogenous H_2O_2 in tumor cells. High concentration of H_2O_2 along with the existence of Fe^{2+} provide a good reactive environment for Fenton Reaction, which drives chemodynamic therapy (CDT) and produces massive reactive oxygen species (ROS) to increase oxidative stress, resulting in tumor cell apoptosis. However, due to the complexity, diversity, and heterogeneity of the tumor microenvironment (TME), the catalytic activity of GOx is limited by hypoxia in the TME, which in turn restricts the further progress of GOx-based cascade reaction.[18,26–29] Poly (lactic-co-glycolic acid) (PLGA) is a bio-degradable and bio-compatible material commonly utilized in drug delivery and controlled release, and it has been approved by the food and drug administration (FDA) for clinical research.[30–32] Ultrasound (US) is a widely-utilized non-invasive tool for diagnosis and treatment in clinic, and it is featured by low energy attenuation and strong tissue penetration ability.[33,34] Low-intensity focused ultrasound (LIFU) is a type of ultrasound which radiates focused ultrasonic wave featured by low-intensity and low-frequency. The dominant function of LIFU is a mechanical effect, due to which microbubbles are forced to vibrate, expand and collapse in

the focused acoustic field.[33,35,36] Furthermore, the focused transducer with high spatiotemporal selectivity guarantees "directional blasting" of diseased tissue and ensures that the ultrasound energy is precisely aligned to the target position, with minimal tissue damage and side effects under repeat treatments.[33,37] Biocompatible liquid perfluorocarbons (PFCs), such as perfluorohexane (PFH), perfluoropentane (PFP) (PFH features higher stability in vivo than PFP due to the higher boiling point), undergo acoustic phase transition and convert from liquid state to gaseous state when stimulated by LIFU, such ultrasonic cavitation effect is also known as acoustic droplet vaporization (ADV) effect.[38–42] Acoustic nanodroplets (NDs) containing liquid cores can convert into microbubbles (MBs) after ultrasound irradiation, followed by MBs rupture due to vibration and expansion, which is termed as ultrasound-targeted microbubble destruction (UTMD).[36] When ADV occurs in tumor region, cellular structure can be affected, inducing blood vessel rupture which eases nanocarriers' penetration through blood vessel-tumor barrier and into internal tumor tissues, and improves the efficacy of anti-tumor therapy.[41–45]

In this study, LIFU-triggered PPFG NPs were designed and synthesized on the basis of the cascade reaction mediated by loading Fe_3O_4/PFH/GOx on PLGA nanocarriers, where PFH (bp ~ 56 °C) was responsible for targeted drug release by ADV effect and providing exogenous oxygen to support GOx-induced tumor starvation, GOx was loaded in the core and adopted to induce tumor starvation by consuming glucose in tumor cells and produce H_2O_2 to provide reactive environment for Fe_3O_4-mediated Fenton reaction, and oleic acid-coated Fe_3O_4 was loaded in the shell and responsible for generating excess ROS and conducting CDT to inhibit tumor growth (**Graphical Abstract**). Non-invasive LIFU not only controls the reaction, but also help impair tumor cells by ADV-effect-caused physically bursting. Such ultrasound-activated phase-change cascade nanoplatform was verified by treating retinoblastoma both in vitro and in vivo, which achieved good biocompatibility and significant anti-tumor effects, providing an alternative solution to address the bottleneck faced by traditional therapies.

Materials and Methods

Materials

Poly (lactic-co-glycolic acid, lactide: glycolide=50:50, Mw=12000Da) (PLGA) was purchased from the Jinan Daigang Biotechnology Company Limited (Shandong, China). Oleic-acid-coated superparamagnetic iron oxide (SPIO) nanoparticles (Fe_3O_4 NPs) (25mg/mL, diameter=5nm) were purchased from Ocean Nano Tech Inc. (Arkansas, USA). Glucose Oxidase (GOx, Purified from Aspergillus niger), Perfluorohexane (PFH, boiling point of 58°C, Mw=338.04) and Poly vinyl alcohol (PVA, Mw = 30,000Da–70,000Da) were obtained from Sigma-Aldrich (USA). The human RB cell line Y79 and human umbilical vein endothelial cells (HUVECs) were purchased from the China Center for Type Culture Collection (Wuhan, China). The Cell Counting kit-8 (CCK-8), Calcein acetoxymethyl (Calcein-AM), and Propidium iodide (PI) were obtained from Dojindo Molecular Technologies (China). Reactive Oxygen Species Assay Kit (2′,7′-dichlorofluorescin diacetate, DCFH-DA), 1.3-diphenylisobenzofuran (DPBF) probes, 1.1′-dioctadecyl-3,3,3′,3′-tetramethylindocarbocyanine perchlorate (DiI) and 4′,6-diamidino-2-phenylindole (DAPI) were acquired from Beyotime Biotechnology (China). All other chemicals were of analytical grade and used without further purification.

Preparation of Nanoparticles

The particles encapsulating GOx, PFH and Fe_3O_4 NPs were prepared by double emulsion method. Firstly, 50mg of PLGA was dissolved in 2mL of dichloromethane (CH_2Cl_2), followed by adding 20μL of Fe_3O_4 NPs and 100μL of GOx solution (5mg of GOx dissolved in 100μL of deionized water). Next, the mixture was emulsified under ice bath by an ultrasonic probe (Sonics & Materials, Inc., USA) after adding PFH (200 μL) as the aqueous phase (2min, 5s ON/5s OFF). Secondly, the emulsified solution was mixed with 5mL of 4% poly vinyl alcohol (PVA) solution and homogenized for the second emulsification (2min,5s ON/5s OFF). After that, 10mL of 2% isopropyl alcohol was added into the emulsion and stirred magnetically for 6h to evaporate dichloromethane. Finally, the solution was centrifuged (10000rpm,5min) and washed with deionized water for three times at 4 °C, and the precipitate was collected and stored at 4 °C for further use. The PLGA-PFH (PP) nanoparticles, PLGA-PFH-Fe_3O_4 (PPF) nanoparticles, PLGA-PFH-GOx (PPG) nanoparticles were prepared in the same way and used as control groups. In addition, the addition of 0.1 mg of DiI to the dissolution of PLGA with CH_2Cl_2 allowed obtaining DiI-labelled corresponding nanoparticles.

Characterization of Nanoparticles

The size distribution and zeta potential of PPFG, PPG (PLGA-PFH-GOx), PPF (PLGA-PFH-Fe_3O_4), PP (PLGA-PFH) nanoparticles were measured by dynamic light scattering (DLS, Malvern Instruments, Malvern, UK). The morphology and structure of PPFG were observed by general microscope (Olympus, Japan), scanning electron microscopy (SEM, Zeiss, Germany), transmission electron microscopy (TEM, Hitachi H-7600, Japan). The optical absorption properties were measured by UV-vis-NIR spectroscope (UV-2550, SHIMADZU, Japan). The encapsulation efficiency and loading content of Fe_3O_4 nanoparticles in PPFG NPs was detected by inductively coupled plasma optical emission spectrometry (ICP-OES). The encapsulation efficiency and loading content of GOx was calculated by high performance liquid chromatography (HPLC).

$$\text{The SPIO encapsulation efficiency}\,(\%) = (\text{total SPIO} - \text{unloaded SPIO})/\text{total SPIO}.$$

$$\text{The SPIO loading content}\,(\%) = (\text{total SPIO} - \text{unloaded SPIO})/\text{total PPFG NPs}.$$

$$\text{The GOx encapsulation efficiency}\,(\%) = (\text{total GOx} - \text{unloaded GOx})/\text{total GOx}.$$

$$\text{The GOx loading content}\,(\%) = (\text{total GOx} - \text{unloaded GOx})/\text{total PPFG NPs}.$$

Nanoparticle Phase Change, Drug Release and ROS Generation

Agar gel model and PPFG nanoparticles at different concentrations were prepared. PPFG was irradiated excited by LIFU (driving frequency: 1 MHz, acoustic intensity: 1.2 W/cm^2, duty cycle: 50%, manufactured by Institute of Ultrasound Imaging of Chongqing Medical University, Chongqing, People's Republic of China), set at different powers (1W, 2W, 3W) for different duration (60s, 120s, 180s, 240s, 270s), respectively. The phase change characteristics were observed by small animal photoacoustic imager in ultrasound mode and contrast enhanced ultrasound development mode. PPFG before/during/after phase change were observed under light microscope. The release of GOx was detected by UV-vis-NIR spectroscope.

The extracellular $^1O_2$ release of all groups (0.5mL, 0.5 mg/mL) with or without LIFU irradiation (3 W, 240s) was assessed by DPBF. Nanoparticles of each group (0.5mL, 0.5 mg/mL) and PBS as the blank control group were added in 48-well plates and treated with 100ul of DPBF (2 mm in ethyl alcohol). After LIFU irradiation (3W, 240 s), the solutions were centrifuged at 10000 rpm for 5 min, and the absorbance of supernatant (DPBF, the absorbance decrease at 415 nm represents the generation of ^{1}O2) was measured by a UV–vis spectrophotometer.

Cell Experiment

Y79 cells and HUVEC cells were cultured in BPMI-1640 medium containing 10% FBS and 1% penicillin–streptomycin under the condition of 37°C and 5% CO_2.

Cell Uptake

Y79 cells were seeded in glass-bottom cell culture dishes (1×10^4 cells per well), and cultured for 12 h. The cell culture medium was disposed and replaced by serum-free medium containing DiI-labeled PPFG nanoparticles (0.5mg/mL), followed by co-incubation for 1 h and 3 h. Then cells were washed thrice with PBS, fixed by 4% paraformaldehyde for 10 min and washed with PBS, and stained by DAPI for 15 min and washed by PBS for three times, and the cellular uptake was observed under confocal laser scanning microscopy (CLSM). The HUVEC cells were set as a control and treated by the same procedure.

Cytotoxicity

The Y79 cells (1×10^4 cells per well) were seeded in 96-well plates after being cultured for 12 h. Then the cells were treated with different nanoparticles (0.5 mg/mL, n=5) and divided into following groups: PBS group, PP group, PPF group, PPG group, PPFG group (PH=7.2), and PPFG group (PH=6.0). CCK-8 assay was applied to evaluate cell viability.

The impact of LIFU irradiation (3 W, 240s) on cell viability was also evaluated. The Y79 cells (1×10^4 cells per well) were seeded in 96-well plates and treated with PPFG nanoparticles at different concentrations (0, 0.0625, 0.125, 0.25, 0.5, and 1mg/mL, n=5) after being cultured for 12h, CCK-8 assay was applied to assess the cell viability of PPFG group, PPFG+LIFU group (PH=7.2), PPFG group (PH=6.0).

Similarity, the cell viability of PPFG+LIFU group (PH=7.2) and PPFG+LIFU group (PH=6.0) (0.5 mg/mL, n=5) was determined by the same method when different concentrations of L-ascorbic acid (0, 5, 10, 20, 40, 80 ug/mL) were added.

In order to visualize the toxicity of nanoparticles to Y79 cells, (Calcein-AM)/(PI) was utilized to label the viable cells/dead cells in the PBS group, LIFU group, PP group, PPF group, PPG group, PPFG+LIFU group (PH=7.2), and PPFG +LIFU group (PH=6.0), respectively, (nanoparticle concentration was set as 1mg/mL). Live cells/dead cells were labeled and incubated for 15 min, the staining solution was removed and rinsed twice with PBS, and then the samples were observed by CLSM.

The cells were treated as aforementioned (1mg/mL) and collected by centrifuge at 1500 rpm for 5 min to further evaluate the cytotoxicity. Apoptosis of Y79 cells were detected by Annexin-fluorescein isothiocyanate/PI labeling and flow cytometry analysis (CytoFLEX, Beckman Coulter, USA).

ROS Generation

The fluorescent substance DCF formed after ROS production in PBS group, LIFU group, PP group, PPF group, PPG group, PPFG group, PPFG+LIFU group (PH=7.2), and PPFG+LIFU group (PH=6.0) (nanoparticle concentration was set as 1mg/mL), was detected by adding DCFH-DA fluorescent probe and observed by CLSM.

Animal Experiment

All animal experiments were authorized by the Animal Ethical Commission of Chongqing Medical University and conducted according to the protocol authorized by the Institutional Animal Care Committee of Chongqing Medical University.

Xenograft Models

Well-grown healthy female BALB/c nude mice (4–6 weeks old, 16–18 g) were purchased and fed in the Animal Center of Chongqing Medical University. Y79 cells (1×10^6 cells) were dissolved in 100μL of PBS (pH=7.2) and injected subcutaneously in the lateral femur of the mice to establish xenotransplantation model of retinoblastoma. Therapies were initiated when the tumors reached a volume of 100 mm^3 [length × $(width)^2/2$].

Anti-Tumor Effect

When the tumor volume of Y79 xenograft reached 100 mm^3, the tumor-bearing mice were randomly divided into seven groups (5mice in each group) and accordingly treated as follows: group 1(control group): saline; group 2: Saline+LIFU; group 3: PP+LIFU; group 4: PPF+LIFU; group 5: PPG+LIFU; group 6: PPFG; group 7: PPFG+LIFU. The concentration of nanoparticles was 5mg/mL, with a dose of 200μL in all groups. LIFU irradiation ($3/cm^2$,240s) was conducted 12h post-injection in groups 2, 3, 4, 5, 7, respectively. Each LIFU irradiation was repeated for four times on the 1st, 3rd, 5th days. The body weights and tumor volumes of the mice were assessed every two days, and the tumor volumes were calculated by following equation: tumor volume = length × $(width^2)/2$.

Histopathological Analysis and in vivo Biosafety

In the end of therapeutic period, the mice were euthanized and the tumors were collected and fixed (4% polyoxymethylene) for histological analysis including hematoxylin–eosin (H&E) staining, TdT-mediated dUTP nick-end labeling (TUNEL), and proliferating cell nuclear antigen (PCNA) staining. Major organs (heart, liver, spleen, lung, and kidney) of the mice were also dissected and fixed with 4% polyoxymethylene for HE staining.

Twenty healthy female BALB/C mice were randomly divided into five groups (n = 4): Control, 1d, 7d, 14d and 21d group. Mice treated with intravenously injection of saline was set as the control group (0 d), and the rest tail intravenous injected with PPFG nanoparticles (5mg/mL) were divided into 1 d, 7 d, 14 d, and 21d groups, and the mice were euthanized at corresponding time points (0d,1d,7d, 14d, and 21d). Blood samples were collected and examined by blood routine examination and blood biochemistry testing in the second affiliated hospital of Chongqing Medical University. The blood routine

examination includes the red blood cell (RBC), white blood cell (WBC), hemoglobin (HGB), mean corpuscular HGB (MCH), mean corpuscular volume (MCV), MCH concentration (MCHC), hematocrit, and platelet (PLT). The biochemistry analysis including the biochemical blood indexes AST, ALT, creatinine, blood urea nitrogen, albumin, and hematological indexes.

Statistical Analysis

All statistical analyses were performed by SPSS 22.0 software (Chicago, IL, USA), and the results are presented as mean ± standard deviations. Comparisons between two groups were assessed with the *t*- test, and one-way analysis of variance (ANOVA) was applied for comparisons among groups. $P < 0.05$ was considered as statistically significant difference. *P < 0.05, **P <0.01, ***P < 0.001, ****P < 0.0001.

Data availability

All the data reported in this work are available upon request.

Results

Synthesis and Characterization of the NPs

PPFG was successfully synthesized by the double-emulsion method, and applied to treat retinoblastoma in vivo and in vitro, which was designed on the basis of adopting PLGA as a nanocarrier to encapsulate PFH and load GOx/SPIO to exploit the cascade reaction between GOx-mediated tumor starvation and CDT induced by SPIO-based Fenton reaction (**Graphical Abstract**).

The average particle size of PPFG stabilized at 255.6nm and the zeta potential stabilized at −27.3 mV (Figure 1A and B). The size and zeta potential of nanoparticles prepared by adding different components (PP, PPF, PPG, PPFG) were shown in Figure 1C. The low polymer dispersibility index (PDI) indicated that the nanoparticles were well dispersed and stable; nanoparticles were all negatively-charged, with a slight increase after Fe_3O_4 was added, which could be due to the positive charge of Fe ions.

The UV absorption characteristics of PP nanoparticles, PPF nanoparticles, PPG nanoparticles, PPFG nanoparticles, and GOx alone are shown in Figure 1D. The absorption peaks of GOx appeared at 382nm and 453nm, which was not detected in nanoparticles containing GOx due to its location in the core of PLGA nanocarriers. In fact, GOx has three absorption peaks, of which 271nm is not shown in the vertical coordinate of the picture in 1D because it is located in the far-ultraviolet region, and the two peaks shown in Figure 1D are located at 382 nm and 453 nm, respectively. Nanoparticles containing different components showed varied light absorption curves at the same concentration. The appearance of nanoparticles containing different components were presented in Figure 1E. The observational results of fluorescence microscope showed that PPFG labeled by DiI were presented as uniform red dots (Figure 1F), which could also be observed under normal optical microscope (Figure S1). The results of SEM demonstrated that PPFG possessed spherical structure with good dispersion (Figure 1G). The TEM image indicated that PPFG showed a shell-core structure, where SPIO was electron-lucent and presented as uniform black dots around the shell and core (Figure 1H and I).

In addition, after incubating the PPFG nanoparticles in both PBS (PH=7.2) and Fetal Bovine Serum (FBS) for 14 days, the particle size barely changed, indicating good stability in FBS (Figure 2A and B).

The encapsulation efficiency and loading content of SPIO was detected to be 84.7±2.5% and 43.07±1.47% by ICP-OES, respectively. The encapsulation efficiency and loading content of GOx was detected to be 33.99±4.19% and 20.72 ±0.95% by HPLC (Figures S2 and S3).

The standard curve of GOx was plotted by measuring the UV absorption spectra of GOx at different concentrations (0.125mg/mL, 0.25mg/mL, 0.5mg/mL), which followed the equation: Y=1.050X+0.04945 with a correlation coefficient of R^2=0.9980 (Figure 2C and D). Based on the standard curve equation, the content of GOx released from PPFG during phase change after LIFU excitation was calculated and the drug release curve was plotted (Figure 2E), according to which the accumulative release rate of GOx reached 79.7967±1.5080% and 81.79±1.4305% under LIFU irradiation (3W) for 240s and 270s, respectively; under irradiation at 1W, the cumulative release rate of GOx was only 16.2667±1.2453% and 17.2567± 1.3333%, respectively; under irradiation at 2W, the cumulative release rate of GOx was 41.2667±1.2684% and 45.26±1.6810%, respectively. The difference in cumulative release rate of GOx under irradiation for 270s was

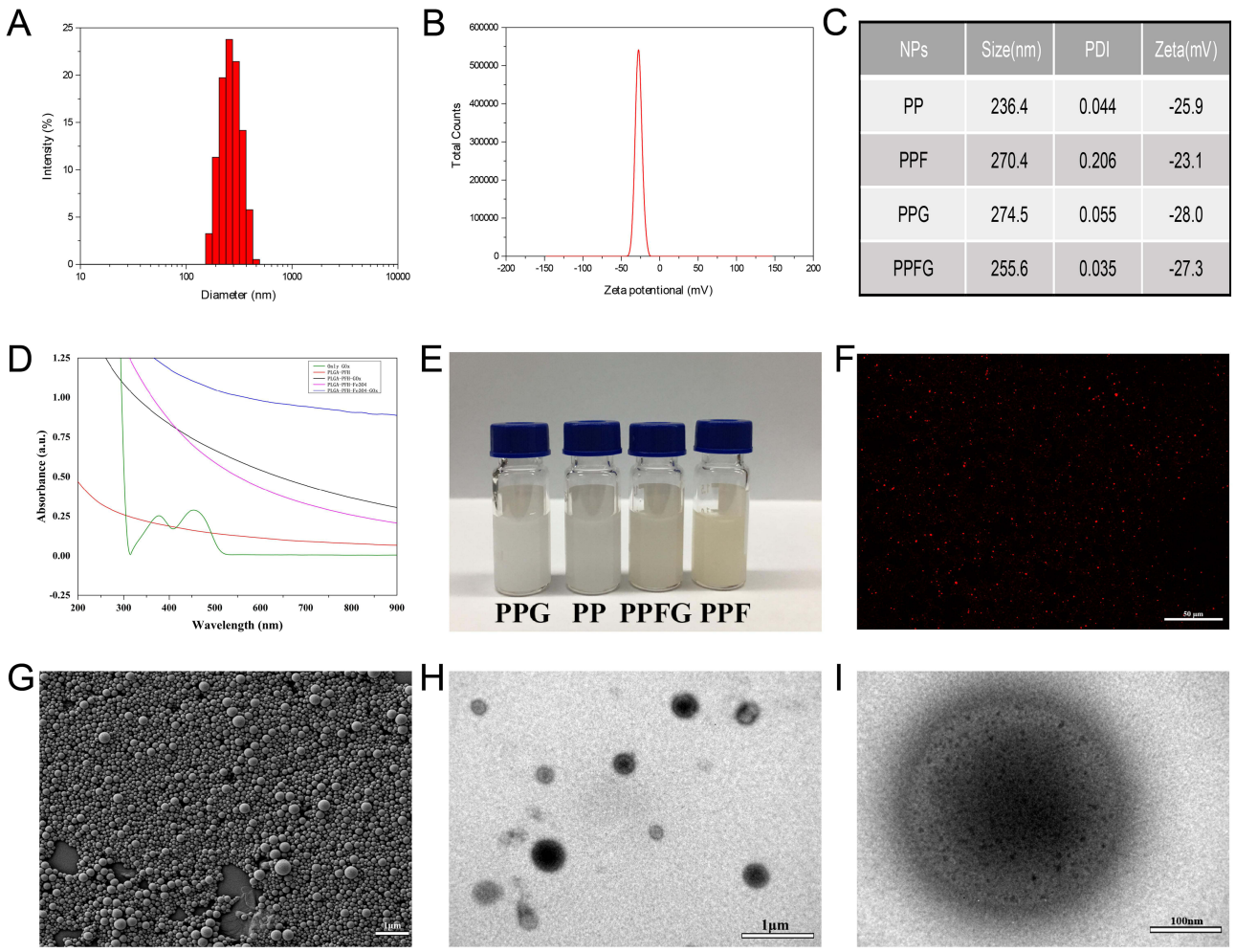

Figure 1 The characterization of PPFG NPs. (**A**) Diameters of PPFG NPs measured by DLS analyzer, (**B**) The zeta potentials of PPFG NPs. (**C**) The Size and zeta of different NPs (PP NPs, PPF NPs, PPG NPs and PPFG NPs) measured by DLS. (**D**) UV–vis spectra of GOx and different NPs (PP NPs, PPF NPs, PPG NPs and PPFG NPs). (**E**) The photographs of the appearance of different NPs (PP NPs, PPF NPs, PPG NPs and PPFG NPs). (**F**) The fluorescence images of the PPFG NPs labelled with Dil. (**G**) SEM image of PPFG NPs. (**H**) and (**I**) TEM image of PPFG NPs at different magnifications.

statistically significant between LIFU power set at 3W and LIFU power set at 2W (P=0.0001), also, the difference between 3W and 1W was statistically significant (P<0.0001), which suggested that PPFG irradiated by LIFU for 270s exhibited the highest release rate of GOx when the irradiation power was set at 3 W. Moreover, no significant difference in the cumulative release rate of GOx was found between the irradiation duration of 240s and 270s (P>0.5) when the power was lower than 3W. To conclude, PPFG exhibited the strongest phase change ability and achieved the highest release rate of GOx under LIFU irradiation for 2min (total time 4min) at 3W.

DPBF probe was utilized to detect ROS generation under different treatment conditions (Figure 2F). The amount of reactive oxygen species can be measured according to the absorbance of DPBF. The DPBF absorbance intensity decreases with the increase of ROS concentration. Notably, the DPBF absorbance intensity in PPFG group under LIFU irradiation decreased dramatically, indicating that PPFG generated higher concentrations of reactive oxygen species under LIFU irradiation. Furthermore, the reactive oxygen species generation capacity was stronger under slightly acidic environment (PH=6.0) compared with neutral environment (PH=7.2). Meanwhile, in the other control groups, the reactive oxygen species generation capacity was lower or even basically did not generate reactive oxygen species. These results suggested that LIFU triggered the drug release of PPFG to generate reactive oxygen species after phase transition.

https://doi.org/10.2147/IJN.S506179

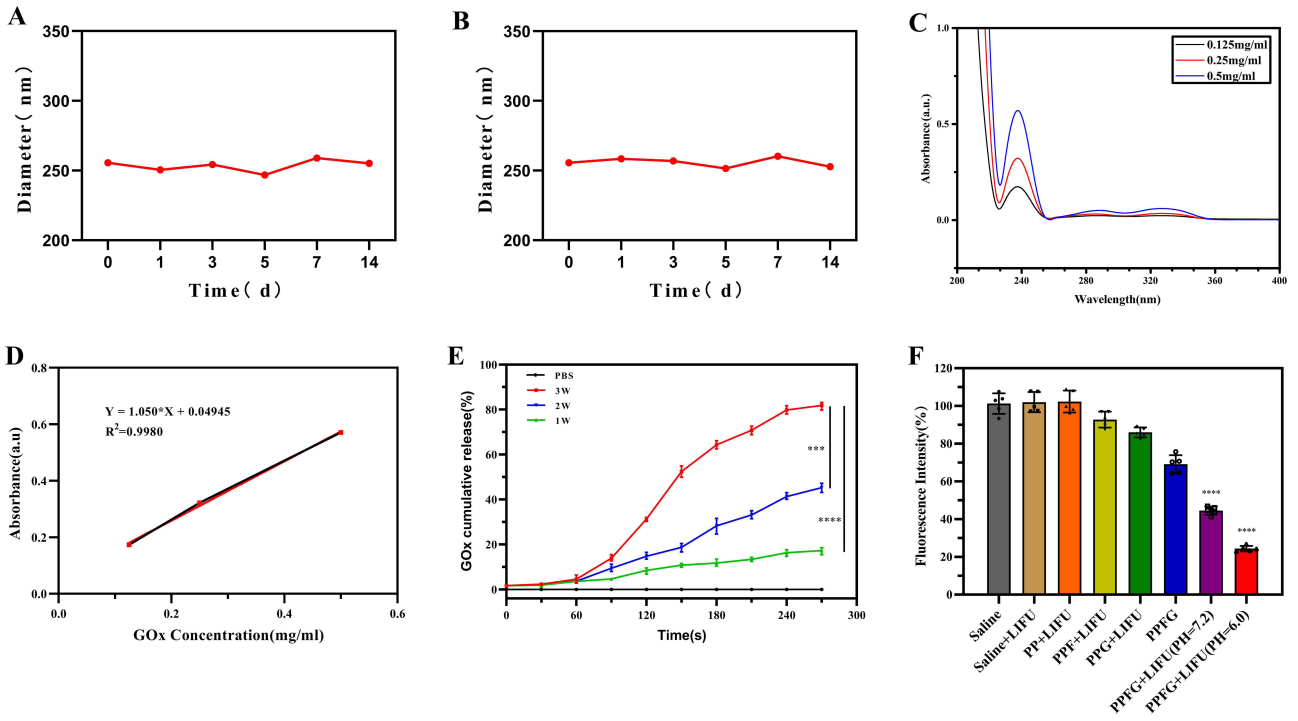

Figure 2 (**A**) and (**B**). The changes of PPFG NPs diameter for 2-week time period in PBS and FBS, respectively. (**C**) The absorbance spectra of GOx at different concentrations (0.125mg/mL,0.25mg/mL and 0.5mg/mL) were measured by UV-vis-NIR spectroscope. (**D**) The relative absorbance intensity of GOx at the wavelength of 237.5 nm. The standard curve of GOx was drawn by the absorbance intensity of GOx at a wavelength of 237.5 nm. (**E**) Cumulative release of GOx from PPFG nanoparticles after exposure to low-intensity focused ultrasound (LIFU) at different powers (1W, 2W and 3W) for different time periods (30s, 60s, 90s, 120s, 150s, 180s, 210s, 240s and 270s), respectively. (**F**) DPBF depletion: the DPBF fluorescence intensity of various nanoparticle groups (0.5mL, 0.5 mg/mL) with or without LIFU exposure (3 W, 240s) was measured by a UV–vis spectrophotometer. (Values are means ± s.d., ***P < 0.001, ****P < 0.0001).

LIFU-Triggered Phase-Changing Ability and Drug Release

The nanoparticles were irradiated by LIFU at different powers, and the echo intensity values were valued in two-dimensional ultrasound (B-Mode) (Table S1) and contrast-enhanced ultrasound (CEUS) (Table S2) at different time points. The results indicated that the echo intensity value of the nanoparticles significantly increased when irradiation power was set at 2W with an effective working duration of 2min, indicating the occurrence of liquid-gas phase transition. When the power was upregulated to 3W with an effective working time of 2min, signal intensity was maximized, where B-Mode and CEUS echo intensity values were detected to be 107.36 ± 5.46db and 85.975 ± 0.455db, respectively. The significant difference in echo value intensity under different power and duration indicated irradiation by LIFU at 3W for 2 min could be considered as effective conditions for the phase transition. In order to visualize the phase transition effect of nanoparticles, PPFG before and after the phase transition was observed under the light microscope (Figures 3A or S1), which showed that the nanoparticles before the phase transition were dot-like, with a uniformly distributed particle size of about 200–300 nm. The particle size of nanoparticles after the phase transition increased significantly to about 100 μm and kept increasing until rupture, and the quantity of nanoparticles undergone phase transition increased as time prolonged (Figure 3A). Meanwhile, Differences before and after the phase transition were reflected not only on particle size, but also on the corresponding echo intensity values in B-Mode and CEUS mode (Figure 3B), where the region of interest (ROI) of the nanoparticles in the B-Mode was significantly enhanced after the phase transition under the LIFU excitation (3W, effective time of 2 min) compared with that before the excitation. The echo intensity value of PPFG nanoparticles was 30.93±7.449db before the phase transition and 110.39±7.573db after the phase transition ($P=0.0108<0.05$, $n=3$), while the difference in the ROI in saline group before/after irradiation was not statistically significant ($P=0.1835$, $n=3$). Situation in CEUS mode was in accordance with that in B-mode, where the intensity was 3.033±0.525db before the phase transition and significantly increased to 81.273±8.156db after the phase transition ($P=0.0034$, $n=3$) (Figure 3C). These results indicated that PPFG was able to undergo phase transition with LIFU irradiation, and nanoparticle size and the echo intensity in B-Mode and CEUS mode significantly increased during the phase transition.

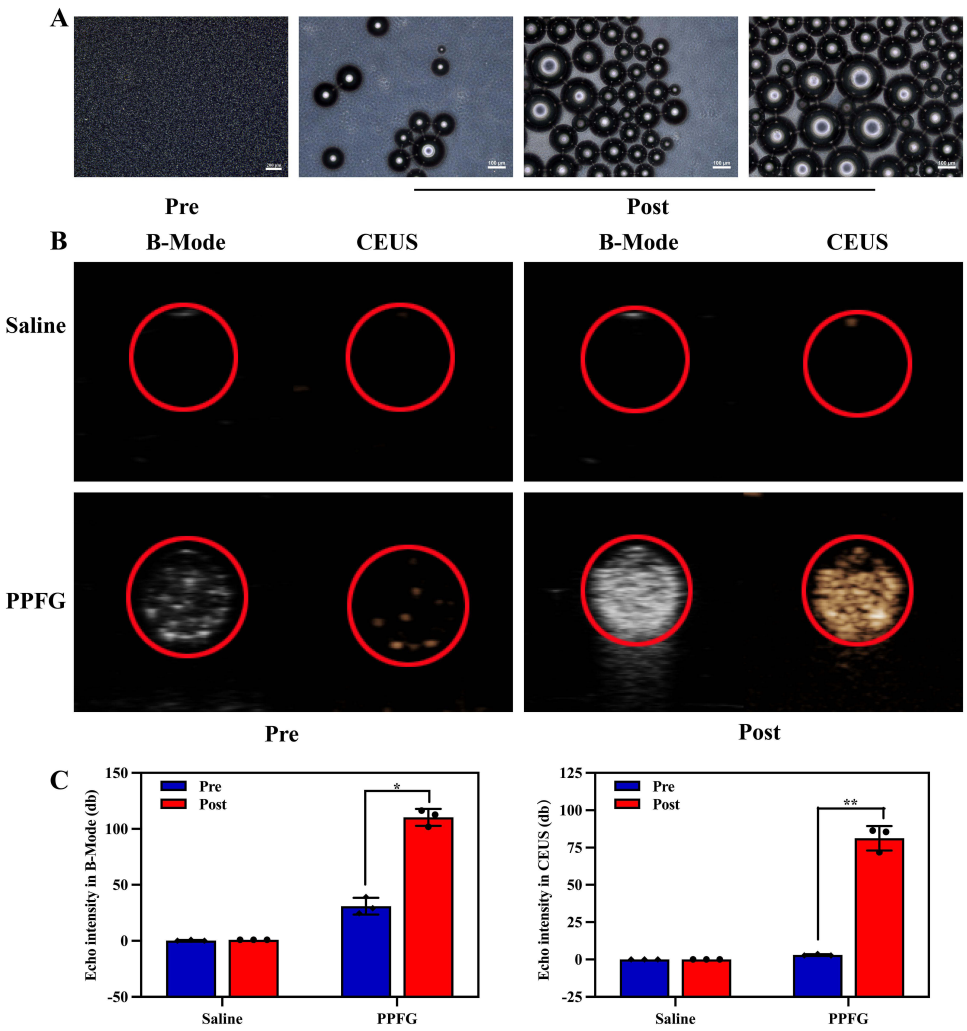

Figure 3 (A) Optical microscopy images of the PPFG NPs before (Pre) and after (Post) LIFU irradiation. (**B**) B-Mode and contrast enhanced ultrasound (CEUS) imaging with Saline and PPFG NPs before and after LIFU irradiation, respectively. (**C**) The echo intensities of the B-Mode and CEUS imaging with Saline and PPFG NPs before and after LIFU irradiation, respectively. Mean values and error bars are defined as mean and s.d., respectively. *P < 0.05, **P < 0.01.

Cell Uptake

The intracellular uptake of PPFG for extended incubation duration (1 and 3 h) was visualized by CLSM) images, and the cellular uptake of PPFG by HUVEC cells was set as the control group. As expected, CLSM observational results showed that PPFG labeled by DiI efficiently accumulated in Y79 cancer cells and the ingestion was almost saturated in 1 hour, while the HUVEC cells ingested much less quantity of PPFG and the ingestion of PPFG exhibited an unapparent increase as time prolonged to 3 hours, which indicated that tumor cells exhibited stronger internalization capacity towards PPFG rather than normal cells (Figure 4).

Cytotoxicity

The cytotoxicity of PPFG to Y79 cancer cells was evaluated by CCK-8 assay. Theoretically, without LIFU irradiation, PPFG should stay in a stable status without any drug release, and exhibit no significant inhibition effect on cell viability within a certain concentration range. Thus, except for the impact of the components on the cytotoxicity of nanoparticles, the concentration, LIFU irradiation and pH were also taken into consideration. As shown in Figure 5A, cell viability of Y79 cells treated by PPFG with LIFU irradiation was lower than that without LIFU irradiation. Meanwhile, Y79 cells treated with PPFG with LIFU irradiation exhibited lower cell viability in a simulated acidic tumor microenvironment. Interestingly, Y79 cells treated with PPFG without LIFU irradiation also exhibited slightly lower cell viability in a simulated acidic tumor microenvironment, which may be due to slight drug release caused by the acidic-

https://doi.org/10.2147/IJN.S506179

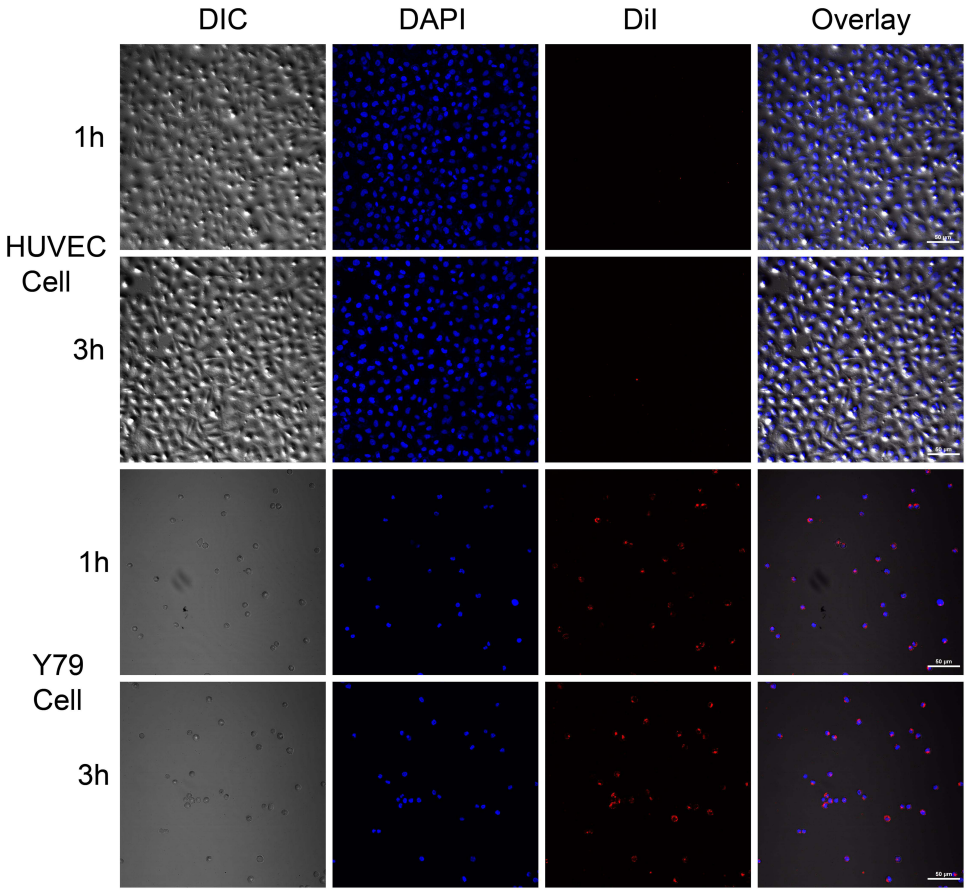

Figure 4 Intracellular uptake of PPFG NPs observed by CLSM after various times (1h and 3h) of incubation with HUVEC Cells and Y79 Cells Through the EPR effect, respectively. The scale bars are 50 μm. DIC indicates bright field. DAPI-labeled nucleus, and DiI-labeled PPFG NPs.

environment-related weakening of nanoparticle stability. As shown in Figure 5B, under LIFU irradiation, with the increase of PPFG nanoparticle concentration, the survival rate of Y79 cells decreased significantly, such situation was even intensified when the environment was acidic, however, Y79 cells remained good viability of 79.420±1.427% when PPFG was applied at a concentration of 1mg/mL without LIFU irradiation. As shown in Figure 5C, with the addition of antioxidant L-ascorbic acid, cell viability was improved, reflecting that LIFU irradiation indeed caused drug release and subsequently weakened cell viability by generating ROS, which can be prevented or restored by adding antioxidant, and the cell viability was positively correlated with the concentration of the added antioxidant.

In order to visualize the live and dead cells, Y79 cancer cells were stained by calcein-AM and PI after co-incubation with multiple kind of nanoparticles at same concentration for 12 hours. Live and dead cells were represented by green and red fluorescence, respectively, and observed by CLSM. According to the CLSM images in Figure 5D, the eight groups (the control, LIFU only, PP, PPF, PPG, PPFG, PPFG+LIFU (PH=7.2), PPFG+LIFU PH=6.0)), cell death was barely observed in the control, LIFU only, PP and PPF group, while cells in PPG and PPFG group emitted green and red fluorescent at almost equivalent ratios, indicating that GOx was slightly released and caused cell death without LIFU irradiation which was in accordance with the data in cytotoxicity detection (Figure 5A). In PPFG+LIFU (PH=7.2), cell death accounted for the major proportion, while almost no live cell was detected in PPFG+LIFU (PH=6.0), indicating that LIFU irradiation significantly promoted drug release and triggered the synergistic effect, and the anti-tumor effect of PPFG was enhanced in an acidic tumor microenvironment.

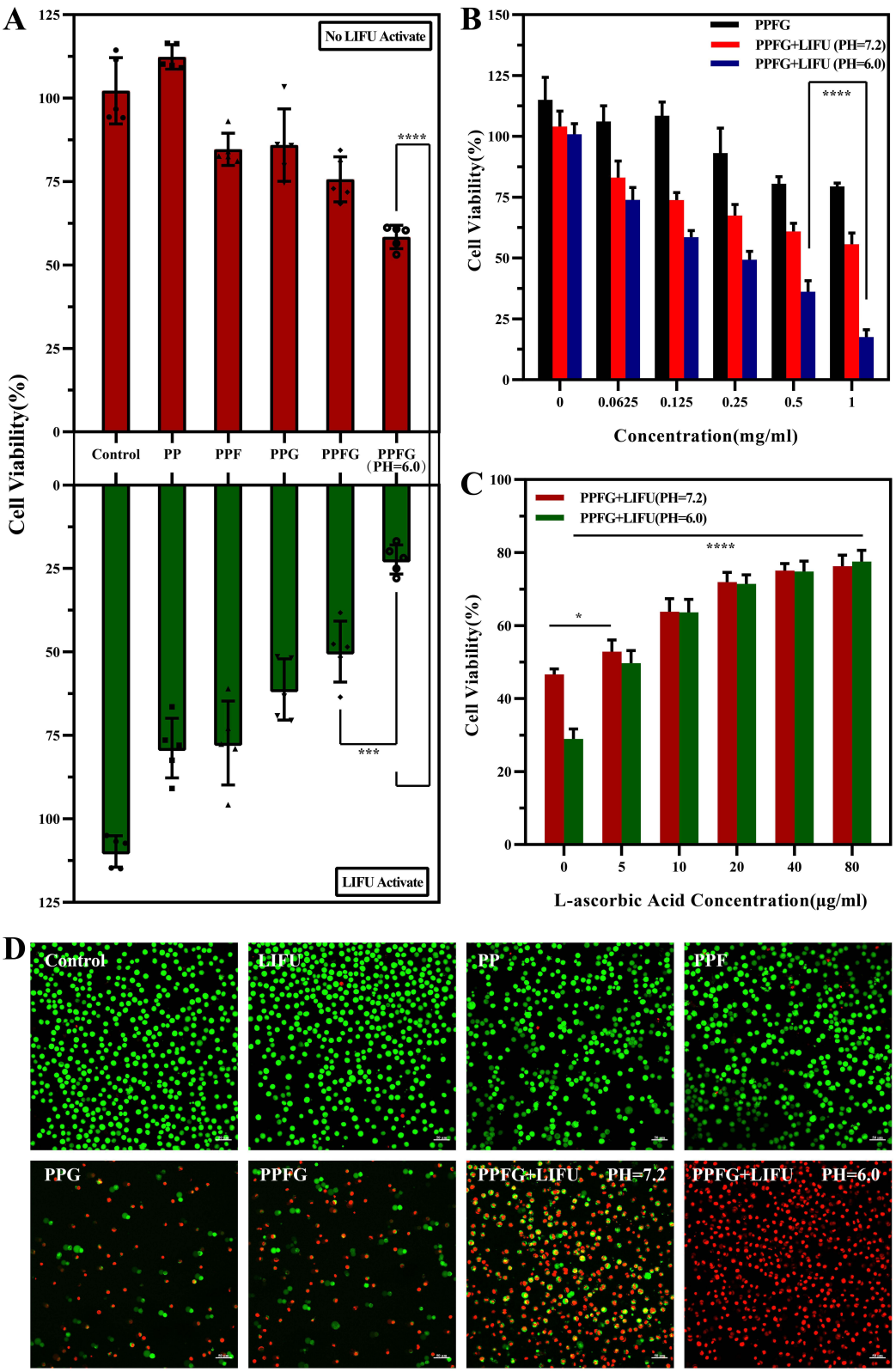

Figure 5 In vitro cytotoxicity of NPs to Y79 cells and intracellular catalytic mechanism. (**A**) Cell viability of Y79 cells after Y79 cells were co-incubated with various nanoparticles or saline and with or without LIFU irradiation was analyzed by CCK-8. (**B**) Cell viability of Y79 cells after co-incubated with different concentration PPFG NPs with or without LIFU irradiation under neutral (pH = 7.2) and acidic (pH = 6.0) conditions. (**C**) Addition of different concentrations of antioxidant L-ascorbic acid rescued PPFG NPs with or without LIFU irradiation under neutral (pH = 7.2) and acidic (pH = 6.0) conditions induced cytotoxicity. (**D**) CLSM images of Calcein-AM and PI co-stained Y79 cells after various treatments (Green: live cells. Red: dead cells). (Mean values and error bars are defined as mean and s.d., respectively. *P < 0.05, ***P < 0.001, ****P < 0.0001. The scale bars are 50 μm).

https://doi.org/10.2147/IJN.S506179

Generation of ROS

The production of reactive oxygen species in the eight groups were detected by DCFH-DA probe, and directly observed under a laser confocal microscope (Figure 6). No ROS production (green fluorescence) was detected in the groups which contained neither GOx nor Fe_3O_4, including control, LIFU only, PP groups; weak signals of ROS were detected in PPF and PPG groups, which could be caused by slight drug release; ROS signal intensity in PPFG group was gradually enhanced, and the ROS production level was maximized in PPFG+LIFU group (PH=6.0), which was also in accordance with the conclusion that LIFU irradiation-caused phase transition of PFH triggered the cascade reaction between the nanoenzyme and CDT especially when the tumor microenvironment was acidic. The fluorescence intensity of reactive oxygen produced by the PPFG+LIFU (PH=6.0) group was about 1.5-fold higher than that of the PPFG+LIFU (PH=7.2) group, 1.8-fold higher than that of the PPFG group, and about 4~5-fold higher than that of the remaining groups (Figure 6I).

Apoptosis Analysis

Apoptosis of Y79 cells was detected by flow cytometry. According to data in Figure 7, cells at the late stage of apoptosis accounted for 90.96% in PPFG+LIFU group (PH=6.0), while cells at the early stage of apoptosis accounted for 6.09%, and the overall apoptosis rate was significantly higher than the other 7 groups, suggesting that the PPFG+LIFU group (PH=6.0) exhibited the strongest toxicity to Y79 tumor cells.

In vivo Therapy

Cancer cells are susceptible to ROS. LIFU, as a non-invasive tool for treating cancer, has significant advantages in tissue penetration and therapeutic precision, which effectively inhibit tumor growth without damaging peripheral healthy tissues. To estimate the therapeutic effect of the LIFU-triggered synergistic reactions by PFH/SPIO/GOx in vivo, Y79 xenograft nude mice were randomly divided into 7 groups according to the corresponding therapeutic scheme, including saline, saline+LIFU, PP+LIFU, PPF+LIFU, PPG+LIFU, PPFG, PPFG+LIFU group (Figure 8). Mice were treated with LIFU irradiation on day 1, 3, 5, and the body weight and tumor volume were measured every two days during the 20-day therapeutic period (Figure 8B and C). As illustrated in Figure 8A, tumor volume in PPFG+LIFU group gradually shrank until it was no longer observable or measurable, while tumor volume in other groups underwent uncontrollable 1.5~3-fold increase or recurrence, indicating that LIFU irradiation, SPIO, and GOx were all essential to the amplified therapeutic effect, and the intimate and reciprocal collaboration among them contributed to the inhibited tumor growth

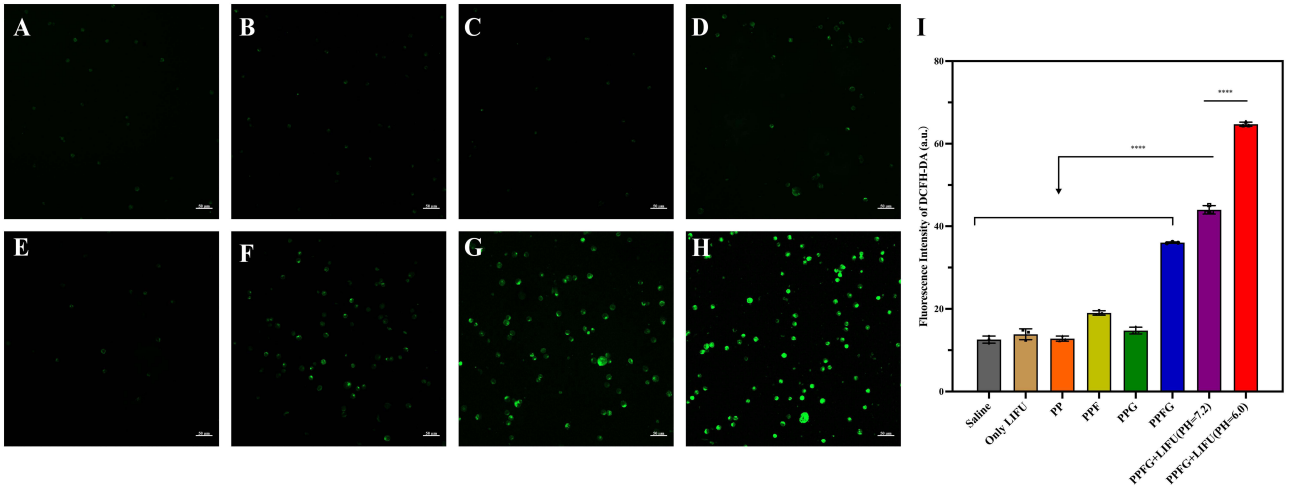

Figure 6 Semi-quantitative CLSM images of ROS production used by ROS fluorescence probe DCFH-DA after Y79 cells were co-incubated with various nanoparticles or saline and with or without LIFU irradiation. (**A**) PBS (control) group. (**B**) Only LIFU group. (**C**) PP group. (**D**) PPF group. (**E**) PPG group. (**F**) PPFG group. (**G**) PPFG+LIFU (PH=7.2) group. (**H**) PPFG+LIFU (PH=6.0) group). (**I**) The fluorescence intensity of ROS with Control group, Only LIFU group, PP group, PPF group, PPG group, PPFG group, PPFG+LIFU (PH=7.2) group and PPFG+LIFU (PH=6.0) group, respectively. (Mean values and error bars are defined as mean and s.d., ****P < 0.0001).

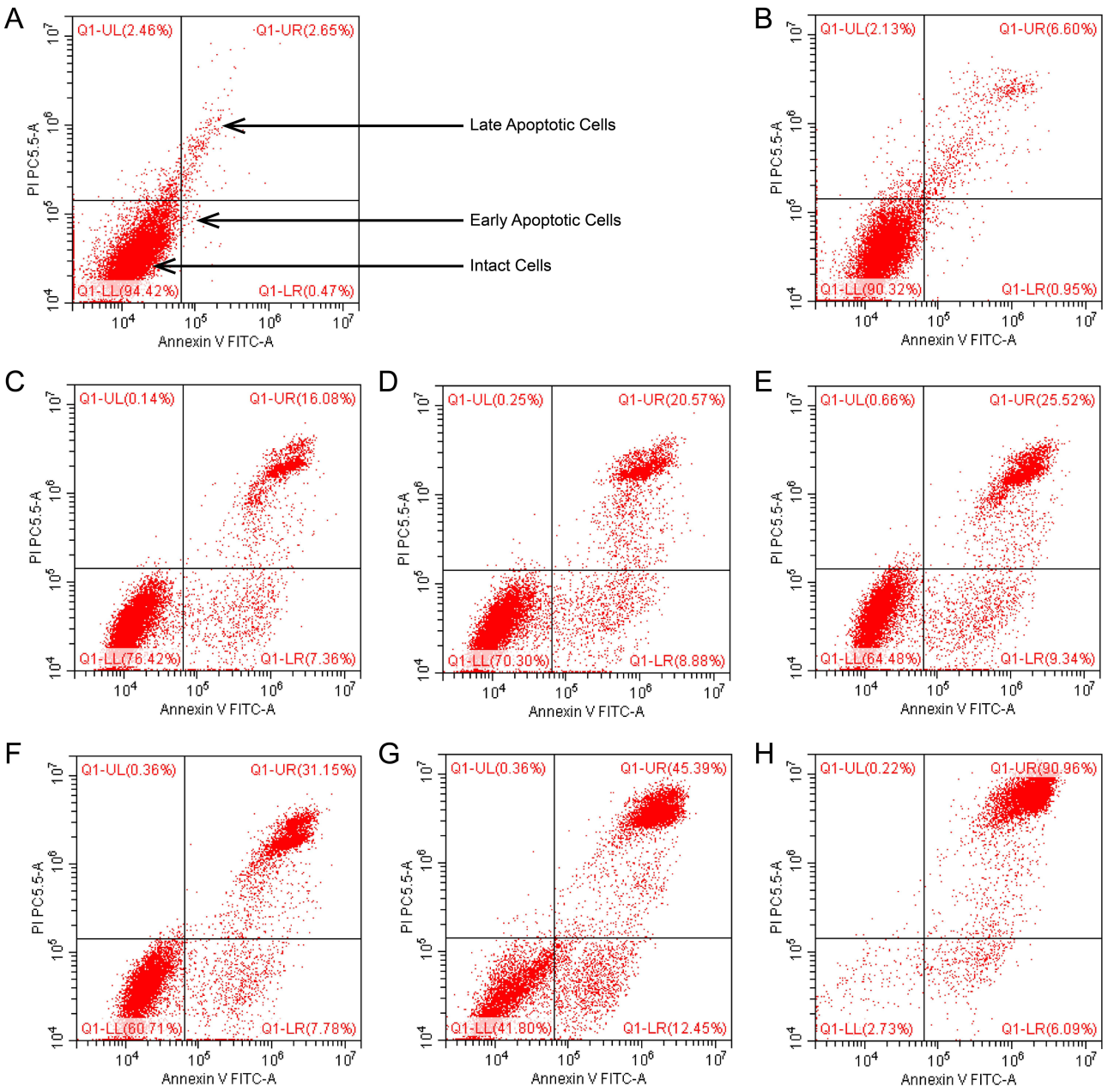

Figure 7 Apoptosis of Y79 cells after different treatments were measured by flow cytometry. (**A**): Control group. (**B**) Only LIFU group. (**C**) PP group. (**D**) PPF group. (**E**) PPG group. (**F**) PPFG group. (**G**) PPFG+LIFU (PH=7.2) group. (**H**) PPFG+LIFU (PH=6.0) group).

in vivo. Additionally, the body weight of mice in all groups was not significantly fluctuated, indirectly suggested that the bio-safety of therapy was confirmed.

H&E, TUNEL and PCNA staining of tumor sections further confirmed the anticancer effect of PPFG+LIFU (Figure 9). H&E staining results showed that apoptosis and necrosis in PPFG + LIFU group were severer compared to that in the other groups. TUNEL assay demonstrated that the fluorescent signal in PPFG + LIFU group was stronger, indicating more tumor cells suffered from injuries, while PCNA results confirmed that the proliferation index in the PPFG + LIFU group was the lowest. These results again confirmed that the PPFG exhibited the highest therapeutic efficacy when triggered by LIFU, and the combination of ultrasound, PFH, SPIO, GOx achieved the therapeutic effect of 1+1+1+1>4.

https://doi.org/10.2147/IJN.S506179

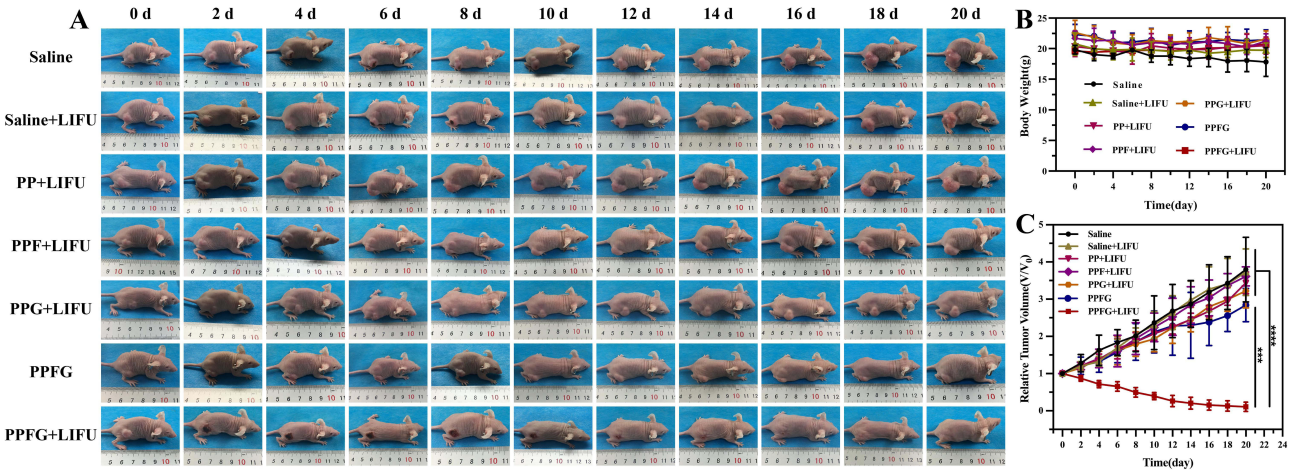

Figure 8 (**A**) Photographs of changes in Y79 tumor-bearing mice of different groups were recorded by cameras every two days during the 20 days. (**B**) The body weight curves of Y79 tumor-bearing mice with various treatments during the 20 days. (**C**) Relative tumor growth curves of seven groups after various treatments during the observation period. (Values are means ± s.d., n = 5, ***P < 0.001, ****P < 0.0001).

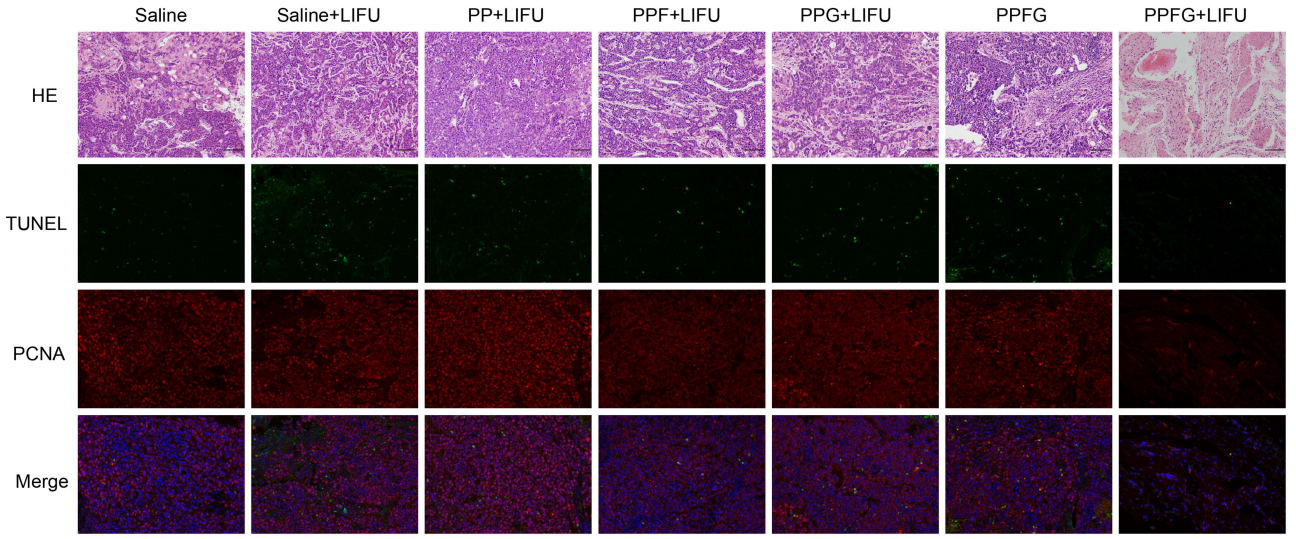

Figure 9 HE, TUNEL, PCNA staining of the tumor tissue at different treatments on the second day after the observation period. From top to bottom: HE-stained cells, TUNEL-positive cells (green), PCNA-positive cells (red), TUNEL and PCNA merge. The DAPI-labeled nuclei is blue. The scale bars are 200 μm.

In vivo Bio-Compatibility

In the end of the treatment, the bio-safety of each treatment group was examined by H&E staining of major organs (heart, liver, spleen, lungs and kidneys) (Figure 10). No significant physiological abnormality was observed in all the groups.

Compared with the control group (0.2 mL, saline), there was no significant changes in blood routine test, including white blood cells (WBC), red blood cells (RBC), platelets (PLT) and other indices (number, morphology, distribution) of PPFG NPs at each time point (Control, 1 d, 7 d, 14 d, 21 d) (Figure 11). Liver function indicators including alanine aminotransferase (ALT), aspartate aminotransferase (AST), alkaline phosphatase (ALP), albumin (ALB), and renal function indicators urea nitrogen (BUN) and serum creatinine (Scr) were within the normal ranges (Figure 11), suggesting that PPFG has no significant side effects on mice.

These results together showed that PPFG caused no significant toxicity in vivo, and good bio-compatibility could facilitate potential clinical translation in the future.

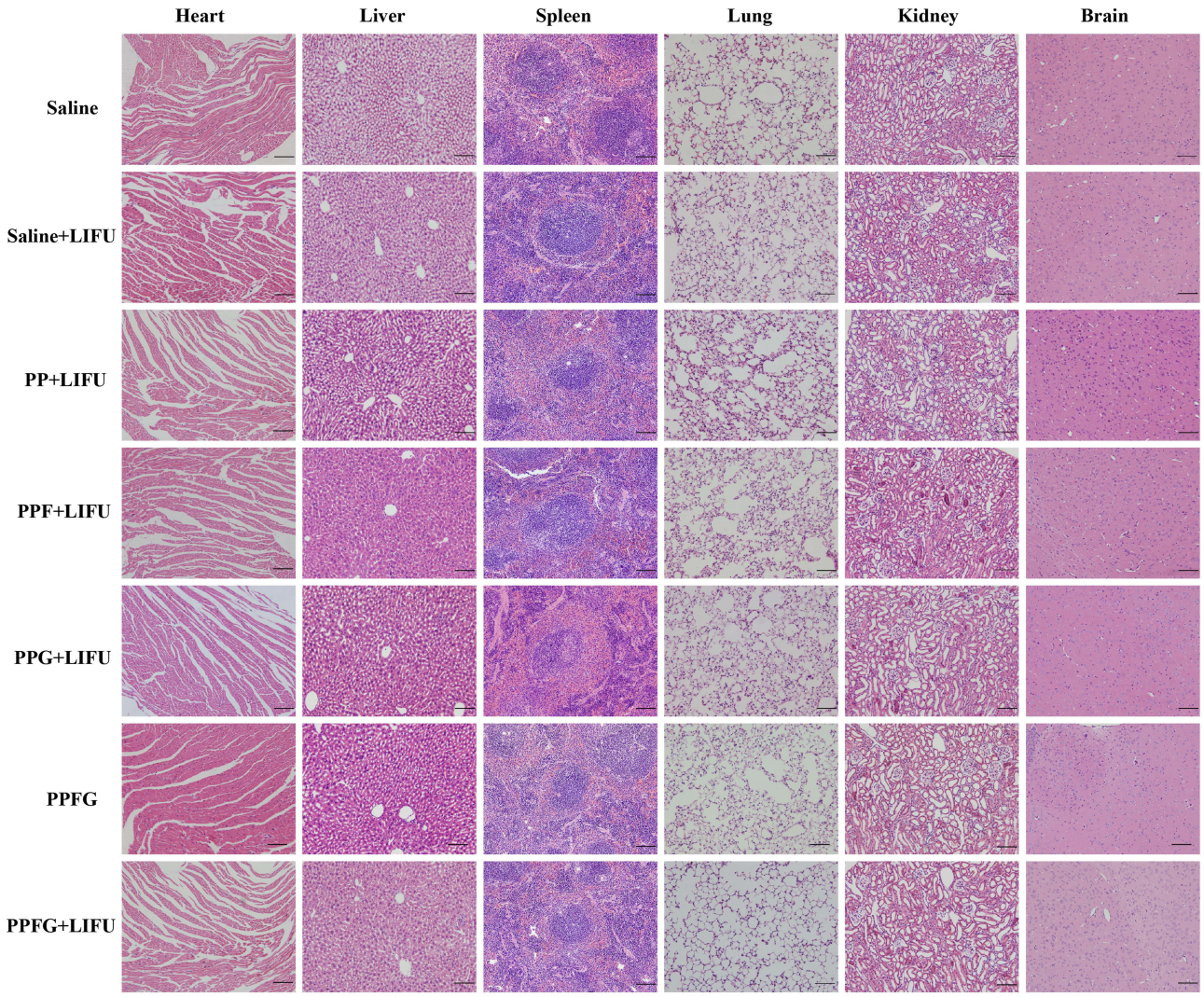

Figure 10 HE staining of the major organs (heart, liver, spleen, lung, kidney and brain) of Y79 tumor-bearing mice after different treatments. The scale bars are 200 μm.

In general, PPFG nanoparticles combined with low-intensity focused ultrasound showed good therapeutic effect in the treatment of retinoblastoma. Although, other nanoparticles (inorganic nanoparticles, lipid nanoparticles) currently investigated for retinoblastoma treatment have superior drug loading capacity or energy conversion capacity, their drawbacks such as long-term biosafety, high cost, and complexity of preparation need to be taken into account.[46] Lipid nanoparticles enable ocular drug delivery through the eye barrier. However, the poor stability limits the application. The polymer organic polymer PLGA has good biocompatibility and stability, the preparation of PPFG nanoparticles is simple, and advanced by low-cost. With LIFU-triggered PFH to generate the ADV effect and UTMD effect to solve the problem of controlled release of drugs, and the intervention of the bioactive enzyme GOx providing a new way in the treatment of retinoblastoma, PPFG+LIFU showed significantly improved therapeutic effect on retinoblastoma. However, there are still many issues to be addressed, for example, 1) the search for nanoparticles with active targeting ability will help to increase cellular uptake and internalisation, and 2) to achieve clinical translation, it is essential to pass through the blood-retinal barrier and blood-aqueous barrier in retinoblastoma in situ, which can be achieved by functionalized nanoparticles (it has been shown that the use of cell-penetrating peptides can increase cellular uptake);[47] 3) deeper enzymatic kinetic reactions could provide additional value for more nanoenzymatic applications in retinoblastoma; 5) real-time monitoring during treatment would be helpful to understand the pathophysiology of retinoblastomas; and 4) metastasis frequently occurs in the advanced stage of retinoblastomas, and

https://doi.org/10.2147/IJN.S506179

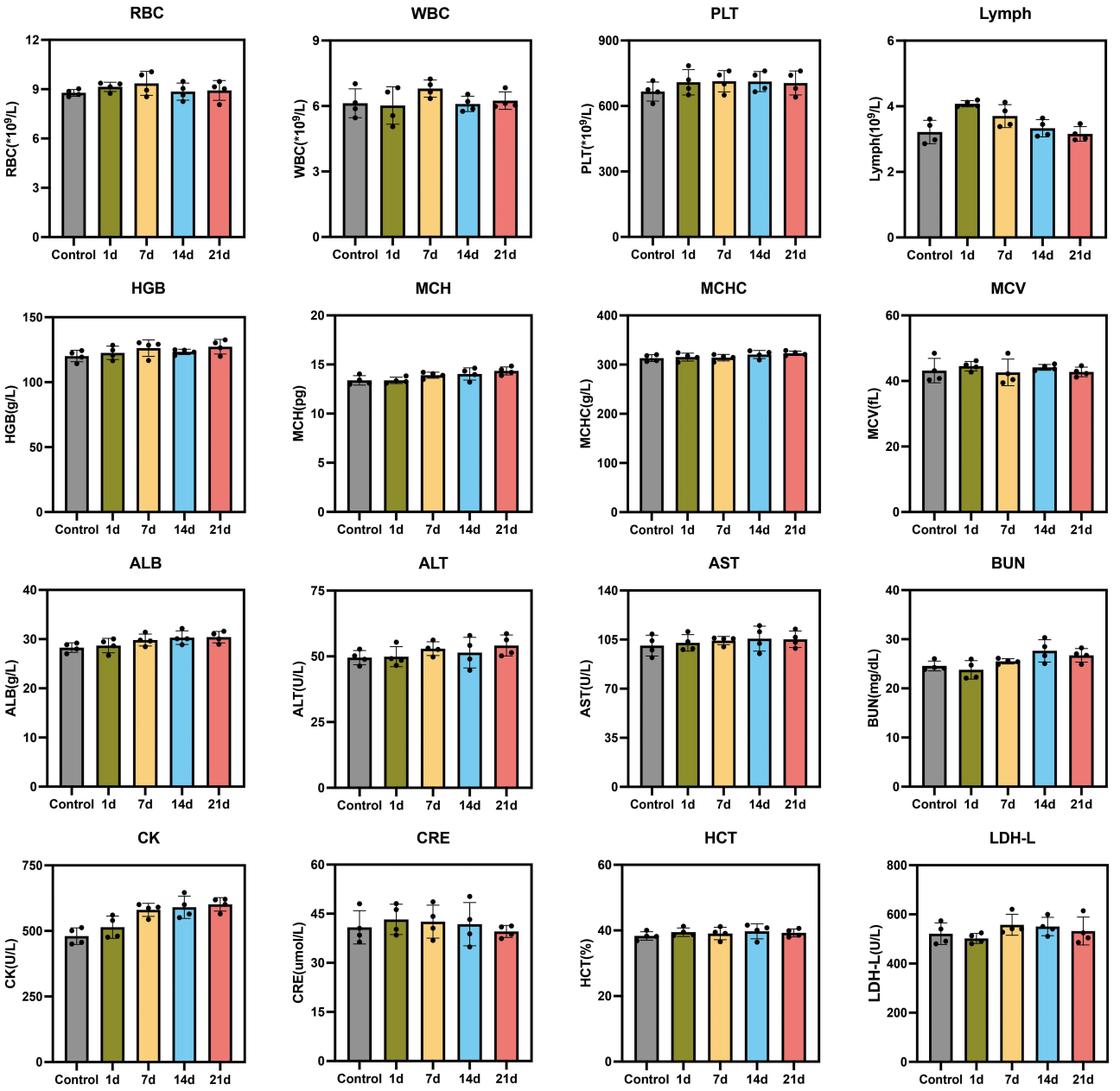

Figure 11 Hematological data and blood biochemical analysis of the treated-mice at control (pre-injection) and 1, 7, 14, and 21 days after-injection with PPFG NPs via the tail vein, including the RBC, WBC and PLT counts, Lymph, HGB, MCH, MCHC, MCV, ALB, ALT, AST, BUN, CK, CRE, HCT and LDH-L levels.

nanoparticles that can be used for both early diagnosis and treatment is of great value. This will be the goal of our subsequent research, and the solution of these problems will provide high value for the clinical translation of nanoparticle-based drug delivery system for retinoblastoma.

Conclusion

In summary, nanozymes have shown unique advantages in anti-tumor therapies. In this study, we successfully constructed an ultrasound-responsive nanozyme-based nanoparticles to treat retinoblastoma, namely PPFG. PPFG targets to tumor in vivo by EPR effect, and realizes ultrasound-responsive drug release by PFH loaded in the core of nanoparticles undergoing liquid-gas phase transition under LIFU irradiation, which can enhance US imaging and improve tumor hypoxia as well. The released GOx efficiently consumes the glucose with the extra supply of oxygen in tumor cells, which impairs tumor cells by causing tumor

starvation, while the reaction product of the glucose oxidase activity H_2O_2 together with Fe_3O_4 mediate Fenton reaction to ultimately generate cytotoxic ROS, such synergy between tumor starvation and chemodynamic therapy achieves significant therapeutic effects on retinoblastoma. Moreover, PPFG possesses high biocompatibility and biosafety, which has been verified in vivo and in vitro. Nonetheless, further investigations on long-term bio-safety examination, the real-time imaging in vivo and the modification of PPFG to gain active tumor-targeting ability would be more evident and beneficial for future clinical application. This study not only has highlighted the significance of the synergistic effect between nanoenzyme-based tumor starvation and CDT, but also laid a good foundation for the development of interdisciplinary therapies for treating retinoblastoma.

Abbreviations

ADV, acoustic droplet vaporization; B-Mode, two-dimensional ultrasound; Calcein-AM, Calcein acetoxymethyl; CCK-8, Cell Counting kit-8; CDT, Chemodynamic therapy; CEUS, contrast-enhanced ultrasound; CLSM, confocal laser scanning microscopy; DAPI, 4′,6-diamidino-2-phenylindole (DAPI); DCFH-DA, 2′,7′-dichlorofluorescin diacetate; DiI, 1.1′-dioctadecyl-3,3,3′,3′-tetramethylindocarbocyanine perchlorate; DPBF, 1.3-diphenylisobenzofuran; EBRT, external beam radiotherapy; EPR, enhanced permeability and retention; FBS, fetal bovine serum; FDA, food and drug administration; GOx, Glucose Oxidase; H&E, hematoxylin–eosin; HPLC, high performance liquid chromatography; HUVEC, human umbilical vein endothelial cell; ICP-OES, inductively coupled plasma optical emission spectrometry; LIFU: low Intensity focused ultrasound; MBs, microbubbles; NDs, nanodroplets; NPs, nanoparticles; PBS, phosphate buffered saline; PCNA, proliferating cell nuclear antigen; PDI, polymer dispersibility index; PFCs, perfluorocarbons; PFH, perfluorohexane; PFP, perfluoropentane; PI, Propidium iodide; PLGA, poly (lactic-co-glycolic acid); PP NPs, PLGA-PFH nanoparticles; PPF NPs, PLGA-PFH-Fe_3O_4 nanoparticles; PPFG NPs, PLGA-PFH-Fe_3O_4-GOx nanoparticles; PPG NPs, PLGA-PFH-GOx nanoparticles; PVA, poly vinyl alcohol; ROI, region of interest; ROS, reactive oxygen species; SEM, scanning electron microscopy; SPIO: superparamagnetic iron oxide; TEM, transmission electron microscopy; TME, tumor microenvironment; TUNEL, TdT-mediated dUTP nick-end labeling; US, ultrasound; UTMD, ultrasound-targeted microbubble destruction.

Acknowledgments

L. Y. Quan and M. Z. Wang contributed equally to this work. This work was supported by the National Natural Science Foundation of China (Grant No.31630026, 81771845, 81630047,1771847,1501482), and the Chongqing Science and Technology Commission (Grant No.cstc2018jcyjAX0562).

Disclosure

The authors report no conflicts of interest in this work.

References

1. Sung H, Ferlay J, Siegel RL, et al. Global Cancer Statistics 2020: GLOBOCAN Estimates of Incidence and Mortality Worldwide for 36 Cancers in 185 Countries. *CA Cancer J Clin*. 2021;71(3):209–249. doi:10.3322/caac.21660
2. Cruz-Galvez CC, Ordaz-Favila JC, Villar-Calvo VM, Cancino-Marentes ME, Bosch-Canto V. Retinoblastoma: review and new insights. *Front Oncol*. 2022;12:963780. doi:10.3389/fonc.2022.963780
3. Dimaras H, Corson TW, Cobrinik D, et al. Retinoblastoma. *Nat Rev Dis Primers*. 2015;1(1):15021. doi:10.1038/nrdp.2015.21
4. Farhat W, Yeung V, Ross A, et al. Advances in biomaterials for the treatment of retinoblastoma. *Biomater Sci*. 2022;10(19):5391–5429. doi:10.1039/d2bm01005d
5. Rao R, Honavar SG. Retinoblastoma. *Indian J Pediatr*. 2017;84(12):937–944. doi:10.1007/s12098-017-2395-0
6. Bhavsar D, Subramanian K, Sethuraman S, Krishnan UM. Management of retinoblastoma: opportunities and challenges. *Drug Deliv*. 2016;23(7):2488–2496. doi:10.3109/10717544.2015.1016193
7. Fabian ID, Onadim Z, Karaa E, et al. The management of retinoblastoma. *Oncogene*. 2018;37(12):1551–1560. doi:10.1038/s41388-017-0050-x
8. Ancona-Lezama D, Dalvin LA, Shields CL. Modern treatment of retinoblastoma: a 2020 review. *Indian J Ophthalmol*. 2020;68(11):2356–2365. doi:10.4103/ijo.IJO_721_20
9. Schaiquevich P, Francis JH, Cancela MB, Carcaboso AM, Chantada GL, Abramson DH. Treatment of Retinoblastoma: what Is the Latest and What Is the Future. *Front Oncol*. 2022;12:822330. doi:10.3389/fonc.2022.822330
10. Fan W, Yung B, Huang P, Chen X. Nanotechnology for Multimodal Synergistic Cancer Therapy. *Chem Rev*. 2017;117(22):13566–13638. doi:10.1021/acs.chemrev.7b00258
11. Russo E, Spallarossa A, Tasso B, Villa C, Brullo C. Nanotechnology for Pediatric Retinoblastoma Therapy. *Pharmaceuticals*. 2022;15(9):1.

12. Mandal M, Banerjee I, Mandal M. Nanoparticle-mediated gene therapy as a novel strategy for the treatment of retinoblastoma. *Colloids Surf B Biointerfaces*. 2022;220:112899. doi:10.1016/j.colsurfb.2022.112899
13. Arshad R, Barani M, Rahdar A, et al. Multi-Functionalized Nanomaterials and Nanoparticles for Diagnosis and Treatment of Retinoblastoma. *Biosensors*. 2021;11(4). doi:10.3390/bios11040097.
14. Li M, Bian X, Chen X, et al. Multifunctional liposome for photoacoustic/ultrasound imaging-guided chemo/photothermal retinoblastoma therapy. *Drug Deliv*. 2022;29(1):519–533. doi:10.1080/10717544.2022.2032876
15. Wang M, Yang Q, Li M, et al. Multifunctional Nanoparticles for Multimodal Imaging-Guided Low-Intensity Focused Ultrasound/Immunosynergistic Retinoblastoma Therapy. *ACS Appl Mater Interfaces*. 2020;12(5):5642–5657. doi:10.1021/acsami.9b22072
16. Zhang X, Chen X, Zhao Y. Nanozymes: versatile Platforms for Cancer Diagnosis and Therapy. *Nanomicro Lett*. 2022;14(1):95. doi:10.1007/s40820-022-00828-2
17. Liang M, Yan X. Nanozymes: from New Concepts, Mechanisms, and Standards to Applications. *Acc Chem Res*. 2019;52(8):2190–2200. doi:10.1021/acs.accounts.9b00140
18. Cai X, Jiao L, Yan H, et al. Nanozyme-involved biomimetic cascade catalysis for biomedical applications. *Mater Today*. 2021;44:211–228. doi:10.1016/j.mattod.2020.12.005
19. Yang Y, Li Z, Fan X, et al. Nanozymes: potential Therapies for Reactive Oxygen Species Overproduction and Inflammation in Ischemic Stroke and Traumatic Brain Injury. *ACS Nano*. 2024;18(26):16450–16467. doi:10.1021/acsnano.4c03425
20. Nn P, Mehla S, Begum A, et al. Smart Nanozymes for Cancer Therapy: the Next Frontier in Oncology. *Adv Healthc Mater*. 2023;12(25):e2300768. doi:10.1002/adhm.202300768
21. Su L, Qin S, Xie Z, et al. Multi-enzyme activity nanozymes for biosensing and disease treatment. *Coord Chem Rev*. 2022;473:214784.
22. He T, Xu H, Zhang Y, et al. Glucose Oxidase-Instructed Traceable Self-Oxygenation/Hyperthermia Dually Enhanced Cancer Starvation Therapy. *Theranostics*. 2020;10(4):1544–1554. doi:10.7150/thno.40439
23. Ren J, Zhang L, Zhang J, et al. Light-activated oxygen self-supplied starving therapy in near-infrared (NIR) window and adjuvant hyperthermia-induced tumor ablation with an augmented sensitivity. *Biomaterials*. 2020;234:119771. doi:10.1016/j.biomaterials.2020.119771
24. Wang R, Yu Y, Gai M, et al. Liposomal Enzyme Nanoreactors based on Nanoconfinement for Efficient Anti-Tumor Therapy. *Angew Chem Int Ed Engl*. 2023;62(44):e202308761. doi:10.1002/anie.202308761
25. Nie C, Pan W, Wu B, et al. Engineered Enzyme-Loaded Erythrocyte Vesicles Precisely Deprive Tumoral Nutrients to Induce Synergistic Near-Infrared-II Photothermal Therapy and Immune Activation. *ACS Nano*. 2023;17(14):13211–13223. doi:10.1021/acsnano.3c00345
26. Fu LH, Qi C, Hu YR, Lin J, Huang P. Glucose Oxidase-Instructed Multimodal Synergistic Cancer Therapy. *Adv Mater*. 2019;31(21):e1808325. doi:10.1002/adma.201808325
27. Wang M, Wang D, Chen Q, Li C, Li Z, Lin J. Recent Advances in Glucose-Oxidase-Based Nanocomposites for Tumor Therapy. *Small*. 2019;15(51):e1903895. doi:10.1002/smll.201903895
28. Liu Q, Zhao Y, Zhou H, Chen C. Ferroptosis: challenges and opportunities for nanomaterials in cancer therapy. *Regen Biomater*. 2023;10:rbad004. doi:10.1093/rb/rbad004
29. Tang Z, Liu Y, He M, Bu W. Chemodynamic Therapy: tumour Microenvironment-Mediated Fenton and Fenton-like Reactions. *Angew Chem Int Ed Engl*. 2019;58(4):946–956. doi:10.1002/anie.201805664
30. Danhier F, Ansorena E, Silva JM, Coco R, Le Breton A, Preat V. PLGA-based nanoparticles: an overview of biomedical applications. *J Control Release*. 2012;161(2):505–522. doi:10.1016/j.jconrel.2012.01.043
31. Lagreca E, Onesto V, Di Natale C, La manna S, Netti PA, Vecchione R. Recent advances in the formulation of PLGA microparticles for controlled drug delivery. *Prog Biomater*. 2020;9(4):153–174. doi:10.1007/s40204-020-00139-y
32. Zhou Y, Yang M, Yan X, et al. Oral Nanotherapeutics of Andrographolide/Carbon Monoxide Donor for Synergistically Anti-inflammatory and Pro-resolving Treatment of Ulcerative Colitis. *ACS Appl Mater Interfaces*. 2023;15(30):36061–36075. doi:10.1021/acsami.3c09342
33. Jiang Z, Xiao W, Fu Q. Stimuli responsive nanosonosensitizers for sonodynamic therapy. *J Control Release*. 2023;361:547–567. doi:10.1016/j.jconrel.2023.08.003
34. Shang L, Yu Y, Jiang Y, et al. Ultrasound-Augmented Multienzyme-like Nanozyme Hydrogel Spray for Promoting Diabetic Wound Healing. *ACS Nano*. 2023;17(16):15962–15977. doi:10.1021/acsnano.3c04134
35. Liu J, You Q, Liang F, et al. Ultrasound-nanovesicles interplay for theranostics. *Adv Drug Deliv Rev*. 2024;205:115176. doi:10.1016/j.addr.2023.115176
36. Cao Y, Chen Y, Yu T, et al. Drug Release from Phase-Changeable Nanodroplets Triggered by Low-Intensity Focused Ultrasound. *Theranostics*. 2018;8(5):1327–1339. doi:10.7150/thno.21492
37. Cao Y, Zhong X, Wu N, et al. An Ultrasound-Responsive and In Situ Gelling Hydrogel Nanocomposite for Boosting Anti PD-L1 Immunotherapy via Remodeling Aberrant ECM of Post-Surgical Residual Cancer. *Adv Funct Mater*. 2024;34(44). doi:10.1002/adfm.202404941.
38. Hou J, Zhou J, Chang M, et al. LIFU-responsive nanomedicine enables acoustic droplet vaporization-induced apoptosis of macrophages for stabilizing vulnerable atherosclerotic plaques. *Bioact Mater*. 2022;16:120–133. doi:10.1016/j.bioactmat.2022.02.022
39. Zhong Y, Zhang Y, Xu J, et al. Low-Intensity Focused Ultrasound-Responsive Phase-Transitional Nanoparticles for Thrombolysis without Vascular Damage: a Synergistic Nonpharmaceutical Strategy. *ACS Nano*. 2019;13(3):3387–3403. doi:10.1021/acsnano.8b09277
40. Xie Z, Wang J, Luo Y, et al. Tumor-penetrating nanoplatform with ultrasound "unlocking" for cascade synergistic therapy and visual feedback under hypoxia. *J Nanobiotechnol*. 2023;21(1):30. doi:10.1186/s12951-023-01765-x
41. Ho YJ, Yeh CK. Theranostic Performance of Acoustic Nanodroplet Vaporization-Generated Bubbles in Tumor Intertissue. *Theranostics*. 2017;7(6):1477–1488. doi:10.7150/thno.19099
42. Kagan D, Benchimol MJ, Claussen JC, Chuluun-Erdene E, Esener S, Wang J. Acoustic droplet vaporization and propulsion of perfluorocarbon-loaded microbullets for targeted tissue penetration and deformation. *Angew Chem Int Ed Engl*. 2012;51(30):7519–7522. doi:10.1002/anie.201201902
43. Zhang L, Yi H, Song J, et al. Mitochondria-Targeted and Ultrasound-Activated Nanodroplets for Enhanced Deep-Penetration Sonodynamic Cancer Therapy. *ACS Appl Mater Interfaces*. 2019;11(9):9355–9366. doi:10.1021/acsami.8b21968
44. Qiu Y, Wu Z, Chen Y, et al. Nano Ultrasound Contrast Agent for Synergistic Chemo-photothermal Therapy and Enhanced Immunotherapy Against Liver Cancer and Metastasis. *Adv Sci*. 2023;10(21):e2300878. doi:10.1002/advs.202300878

45. Zhu L, Zhao H, Zhou Z, et al. Peptide-Functionalized Phase-Transformation Nanoparticles for Low Intensity Focused Ultrasound-Assisted Tumor Imaging and Therapy. *Nano Lett*. 2018;18(3):1831–1841. doi:10.1021/acs.nanolett.7b05087
46. Onugwu AL, Ugorji OL, Ufondu CA, et al. Nanoparticle-based delivery systems as emerging therapy in retinoblastoma: recent advances, challenges and prospects. *Nanoscale Adv*. 2023;5(18):4628–4648. doi:10.1039/D3NA00462G
47. Jiang K, Fan X, Hu Y, et al. Topical instillation of cell-penetrating peptide-conjugated melphalan blocks metastases of retinoblastoma. *Biomaterials*. 2022;284:121493. doi:10.1016/j.biomaterials.2022.121493